

Article

# Multi-Algorithm Indices and Look-Up Table for Chlorophyll-a Retrieval in Highly Turbid Water Bodies Using Multispectral Data

Salem Ibrahim Salem <sup>1,2,\*</sup>, Hiroto Higa <sup>3</sup>, Hyungjun Kim <sup>1</sup>, Komatsu Kazuhiro <sup>4</sup>, Hiroshi Kobayashi <sup>5</sup>, Kazuo Oki <sup>1</sup> and Taikan Oki <sup>1</sup>

<sup>1</sup> Institute of Industrial Science, The University of Tokyo, 4-6-1 Komaba, Meguro-ku, Tokyo 153-8505, Japan; hjkim@iis.u-tokyo.ac.jp (H.K.); kazu@iis.u-tokyo.ac.jp (K.O.); taikan@iis.u-tokyo.ac.jp (T.O.)

<sup>2</sup> Faculty of Engineering, Alexandria University, Lotfy El-Sied St. Off Gamal Abd El-Naser-Alexandria, Alexandria 11432, Egypt

<sup>3</sup> Faculty of Urban Innovation, Yokohama National University, Tokiwadai 79-5, Hodogaya, Yokohama, Kanagawa 240-8501, Japan; higa-h@ynu.ac.jp

<sup>4</sup> National Institute for Environmental Studies, 16-2 Onogawa, Tsukuba, Ibaraki 305-8506, Japan; Kkomatsu@nies.go.jp

<sup>5</sup> Graduate School of Interdisciplinary Research, University of Yamanashi, 4-4-37 Takeda, Kofu, Yamanashi 400-8510, Japan; kobachu@yamanashi.ac.jp

\* Correspondence: salem@rainbow.iis.u-tokyo.ac.jp or eng.salemsalem@gmail.com

Academic Editor: Xiaofeng Li

Received: 14 April 2017; Accepted: 31 May 2017; Published: 3 June 2017

**Abstract:** Many approaches have been proposed for monitoring the eutrophication of Case 2 waters using remote sensing data. Semi-analytical algorithms and spectrum matching are two major approaches for chlorophyll-a (Chla) retrieval. Semi-analytical algorithms provide indices correlated with phytoplankton characteristics, (e.g., maximum and minimum absorption peaks). Algorithms' indices are correlated with measured Chla through the regression process. The main drawback of the semi-analytical algorithms is that the derived relation is location and data limited. Spectrum matching and the look-up table approach rely on matching the measured reflectance with a large library of simulated references corresponding to wide ranges of water properties. The spectral matching approach taking hyperspectral measured reflectance as an input, leading to difficulties in incorporating data from multispectral satellites. Consequently, multi-algorithm indices and the look-up table (MAIN-LUT) technique is proposed to combine the merits of semi-analytical algorithms and look-up table, which can be applied to multispectral data. Eight combinations of four algorithms (i.e., 2-band, 3-band, maximum chlorophyll index, and normalized difference chlorophyll index) are investigated for the MAIN-LUT technique. In situ measurements and Medium Resolution Imaging Spectrometer (MERIS) sensor data are used to validate MAIN-LUT. In general, the MAIN-LUT provide a comparable retrieval accuracy with locally tuned algorithms. The most accurate of the locally tuned algorithms varied among datasets, revealing the limitation of these algorithms to be applied universally. In contrast, the MAIN-LUT provided relatively high retrieval accuracy for Tokyo Bay ( $R^2 = 0.692$ , root mean square error (RMSE) =  $21.4 \text{ mg m}^{-3}$ ), Lake Kasumigaura ( $R^2 = 0.866$ , RMSE =  $11.3 \text{ mg m}^{-3}$ ), and MERIS data over Lake Kasumigaura ( $R^2 = 0.57$ , RMSE =  $36.5 \text{ mg m}^{-3}$ ). The simulated reflectance library of MAIN-LUT was generated based on inherent optical properties of Tokyo Bay; however, the MAIN-LUT also provided high retrieval accuracy for Lake Kasumigaura. MAIN-LUT could capture the spatial and temporal distribution of Chla concentration for Lake Kasumigaura.

**Keywords:** bio-optical model; Red-NIR algorithm; Case 2 waters; inland lakes; MERIS; look-up table; spectral matching

## 1. Introduction

Ocean color satellites have provided synoptic observation for oceans, coastal areas and inland water bodies [1,2]. Coastal Zone Color Scanner (CZCS) was the first ocean color satellite, which enables the ocean community to map the spatial distribution of ocean properties [3], such as the diffuse attenuation coefficient [4] and chlorophyll-a (Chla) concentration [5]. After a gap of 10 years from the end of CZCS mission, the Sea-viewing Wide Field-of-view Sensor (SeaWiFS) was launched in 1997. Since then, continuous monitoring of water bodies is achieved through many satellites [6,7]. Most of these satellites provided multispectral data with reasonable spatial and temporal resolution [8], and it is freely available [9,10]. Monitoring of Chla concentration in Case 1 waters (e.g., open oceans) using satellite sensors has been established due to the fact that the phytoplankton is governing the optical properties [11,12]. Several approaches were developed for Case 1 waters such as quasi-analytical algorithm (QAA) [13], the Garver–Siegel–Maritorena (GSM) algorithm [14], and the band ratio in the blue-green wavelengths as ocean color V4 (OC4E) algorithm [15]. Both QAA and GSM derive inherent optical properties of open oceans, while the difference between them is that GSM requires the absorption spectral shape of water constituents, while QAA does not require these data [16].

Chla retrieval accuracy for Case 2 waters using in situ or satellite data is a challenging problem due to the complex interaction between Chla, non-algal particles (NAP), and colored dissolved organic matter (CDOM) [17–19]. A lot of effort has been made to overcome that complexity, resulting in several approaches have been proposed, including bands ratio [20–23], semi-analytical algorithms [24–26], semi-analytical inversion/optimization approach [27–30], spectrum matching and look-up tables [31,32], and neural network (NN) [33–35]. Empirical and semi-analytical algorithms provide indices that are correlated with Chla concentration [23,36–38]. The retrieval of Chla concentration from algorithm's indices is achieved through regression processes using linear [39–42], polynomial [36,43,44], and power regression approaches [15,45]. Matthews [46] reviewed the retrieval accuracy of many algorithms for different sites, revealing the ability of tuned algorithms to retrieve Chla concentration. However, the main limitation associated with the empirical and semi-analytical algorithms is that the derived relationship may not be applicable to other locations with different water composition [47].

Lee et al. [48] developed a semi-analytical inversion model for shallow water to derive water depth, and water column properties (i.e., absorption and backscattering coefficients) of the water column by optimizing the difference between measured reflectance ( $R_{rs}$ ) and simulated  $R_{rs}$ . Many researchers upgraded the model of Lee et al. [48] to involve many bottom types instead of sand-bottom type [28,49] and to retrieve Chla, NAP, and CDOM concentrations [30]. These inversion models were mainly applied to shallow, and relatively clear water with high CDOM concentrations in the Bahamas and Moreton Bay in eastern Australia using airborne hyperspectral data with a high spatial resolution [50–53]. The airborne hyperspectral data is much more expensive with small area coverage compared with multispectral satellite dates that are freely available for many satellites with routine global coverage [54]. Regarding spectrum matching approach, a matchup process is performed between the measured  $R_{rs}$  and a library of simulated  $R_{rs}$  covering different water conditions to find the closest simulated  $R_{rs}$  with its known properties [55]. Similarly, a spectrum matching approach requires hyperspectral data to perform the matching process.

Accordingly, a new technique is required to combine the advantages of semi-analytical algorithms (i.e., providing indices correlated with Chla concentration) with the merits of the look-up table (i.e., providing dataset corresponding to various water properties) and applicability to multispectral data. The current study proposed multi-algorithm indices and the look-up table technique. The aim of this study is to (1) develop a new technique for Chla retrieval based on algorithms' indices and look-up tables; (2) select the proper combination of algorithms for the proposed technique; and (3) evaluate the performance of proposed technique using in situ measurements and Medium Resolution Imaging Spectrometer (MERIS) sensor data over turbid and highly turbid water bodies.

## 2. Methods

### 2.1. In Situ and Laboratory Measurements

Data collected from Tokyo Bay ( $35^{\circ}25'N$ ;  $139^{\circ}47'E$ ), and Lake Kasumigaura ( $36^{\circ}03'N$ ;  $140^{\circ}25'E$ ) were used to validate the proposed technique (Figure 1). In situ remote sensing reflectance spectra along with water quality parameters (e.g., Chla concentrations) were collected for Tokyo Bay from June 2010 to August 2013 (sixteen campaigns) and for Lake Kasumigaura in 2016 (eight campaigns). Figure 2 illustrates the remote sensing reflectance spectra for both sites. The red reflectance spectra shown in Figure 2b represent 12 stations of Tokyo Bay where additional inherent optical measurements (i.e., absorption and backscattering coefficients) were executed. Furthermore, water quality parameters were also collected monthly since 1977 by the National Institute for Environmental Studies (NIES) [56]. Monthly campaigns of NIES were compared with acquired MERIS data to extracted matched dates, resulting in 77 stations. Table 1 summarized the basic characteristics of collected data, revealing that Lake Kasumigaura is a highly turbid water body comparing with Tokyo Bay. The Chla concentrations were fluorometrically measured using a Turner Designs 10-AU fluorometer [57]. A 20 mL of water samples was filtered through 25-mm Whatman GF/F filters of a  $0.7\text{-}\mu\text{m}$  pore size, then the pigments were extracted by soaking the filter in 6 mL of *N,N*-dimethylformamide (DMF) and storing it in dark at  $4\text{ }^{\circ}\text{C}$  for 4 h [58]. The total suspended solids (TSS), organic suspended solids (OSS), and inorganic suspended solids (ISS) were determined gravimetrically [59].

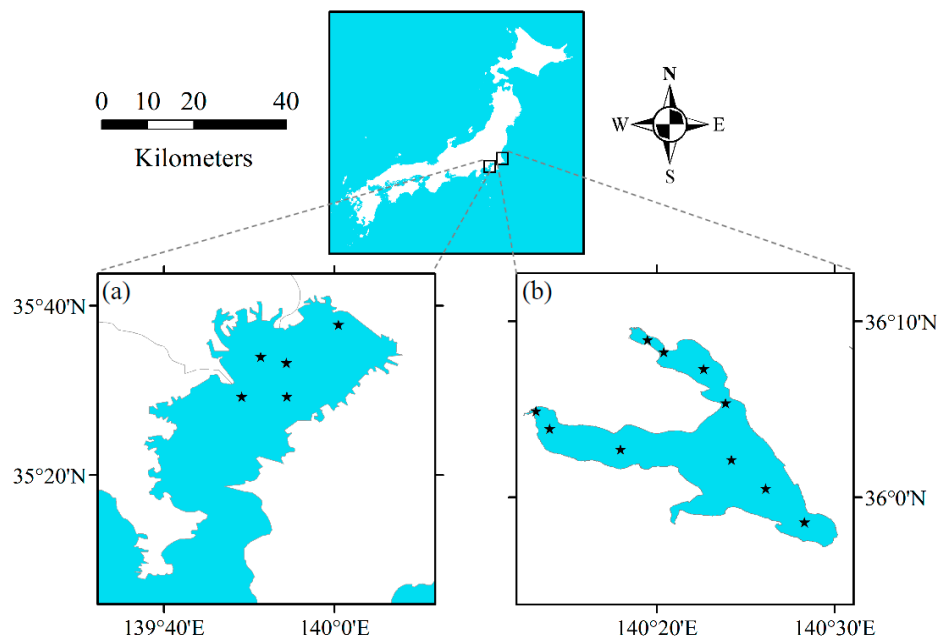


**Figure 1.** Location of the sampling sites. (a) Tokyo Bay; and (b) Lake Kasumigaura.

In situ remote sensing reflectance spectra were collected using two different instruments: (1) three TriOS-RAMSES hyperspectral radiometers (Oldenburg, Germany) in the spectral range between 350 nm and 900 nm at a 2 nm spectral interval and a field-of-view of  $7^{\circ}$  used for Tokyo Bay field observation, and (2) FieldSpec HandHeld 2 Spectroradiometer (Boulder, CO, USA) in the spectrum range from 350 to 1075 nm with spectral resolution of 1.0 nm and  $25^{\circ}$  field-of-view used for Lake Kasumigaura. The protocol proposed by Mobley [60] was adopted for HandHeld 2. The absorption coefficients of phytoplankton, non-algal particles, and colored dissolved organic matter were measured with the quantitative filter technique (QFT) approach [61] using a UV/VIS spectrophotometer (JASCO, V550, Hachioji, Japan). The vertical profiles of the total backscattering coefficients ( $b_b(\lambda)$ ) were measured at six wavelengths (420, 442, 488, 510, 550 and 676 nm) with a HydroScat-6 (HOBI Labs Inc., Tucson, AZ,

USA). The backscattering coefficients for particles were estimated by subtracting the backscattering of pure water [62,63] from the total backscattering coefficients ( $b_b(\lambda)$ ) [64].

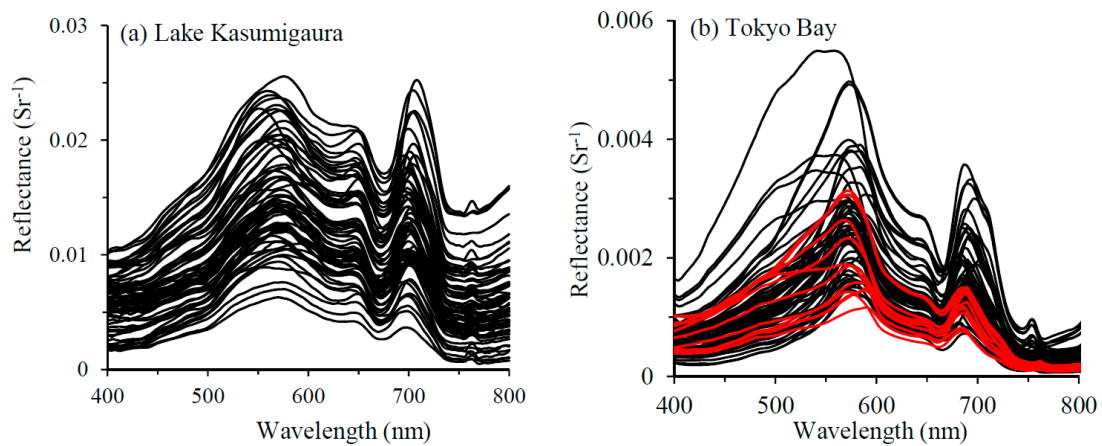


**Figure 2.** Remote sensing reflectance collected from (a) Lake Kasumigaura and (b) Tokyo Bay. The red lines highlighted the 12 stations of Tokyo Bay that had additional measurements of absorption and backscattering properties along with remote sensing reflectance measurements.

**Table 1.** Descriptive statistics of the water quality parameters for Tokyo Bay, and Lake Kasumigaura. *Tokyo Bay with IOPs* (inherent optical properties) dataset refers to stations where additional measurements of absorption and backscattering properties were performed along with remote sensing reflectance measurements. Lake Kasumigaura *Datasets 1* and *2* represent measurements collected in 2016 and during 2002–2012, respectively.

	Min	Max	Mean	Median	SD	RSD (%)
Tokyo Bay ( $n = 71$ )						
Chla ( $\text{mg m}^{-3}$ )	0.76	102.07	25.14	13.94	25.85	102.82
TSS ( $\text{g m}^{-3}$ )	2.99	26.29	8.29	7.99	0.49	5.87
Tokyo Bay with IOPs ( $n = 12$ )						
Chla ( $\text{mg m}^{-3}$ )	2.9	42.6	18.31	11.85	14.99	81.87
TSS ( $\text{g m}^{-3}$ )	2.99	9.86	6.34	6.81	2.24	35.38
ISS ( $\text{g m}^{-3}$ )	0.81	6.13	2.96	2.22	1.63	55.24
OSS ( $\text{g m}^{-3}$ )	0.96	7.16	3.39	2.9	1.75	51.63
$a_{ph}(440)$ ( $\text{m}^{-1}$ )	0.23	1.03	0.65	0.6	0.27	41.3
$a_{NAP}(440)$ ( $\text{m}^{-1}$ )	0.14	0.34	0.22	0.21	0.07	31.75
$a_{CDOM}(440)$ ( $\text{m}^{-1}$ )	0.06	0.47	0.25	0.19	0.14	56.23
$b_{b,p}(442)$ ( $\text{m}^{-1}$ )	0.01	0.04	0.02	0.03	0.01	41.16
Lake Kasumigaura (Dataset 1) ( $n = 68$ )						
Chla ( $\text{mg m}^{-3}$ )	13.16	152.14	55.86	48.16	26.59	47.60
TSS ( $\text{g m}^{-3}$ )	9.40	57.10	21.71	18.25	9.44	43.50
Lake Kasumigaura * (Dataset 2) ( $n = 77$ )						
Chla ( $\text{mg m}^{-3}$ )	8.10	179.40	65.98	59.90	35.90	54.42
TSS ( $\text{g m}^{-3}$ )	10.70	59.10	25.00	23.67	10.14	40.56

\* Data was collected by the National Institute for Environmental Studies (NIES). Chla refers to chlorophyll-a concentration; TSS, ISS and OSS stand for total, inorganic and organic suspended solids, respectively;  $a_{ph}(440)$ ,  $a_{NAP}(440)$  and  $a_{CDOM}(440)$  represent the measured absorption coefficients for phytoplankton, non-algal particles (NAP), and colored dissolved organic matter (CDOM) at 440 nm bands, respectively;  $b_{b,p}(442)$  denotes the measured backscattering at 442 nm bands;  $n$  represents the number of samples; SD stands for standard deviation; and RSD denotes relative standard deviation =  $(\text{SD}/\text{Mean} \times 100)$ .

## 2.2. Bio-Optical Model

Subsurface remote sensing reflectance ( $r_{rs}(\lambda)$ , all symbols are defined in Table 2) was fitted with inherent optical properties (IOPs) using polynomial function by Gordon et al. [65], which can be simplified as

$$r_{rs}(\lambda) = \frac{f}{Q} \times \left( \frac{b_b(\lambda)}{a(\lambda) + b_b(\lambda)} \right) \quad (1)$$

where  $f$  is the light field factor; and  $Q$  denotes the light distribution factor. Kirk [66] found that  $f$  is a function of the solar altitude, which is expressed as a linear function of the cosine of the zenith angle of the refracted photons  $\mu_0$ :

$$f = 0.975 - 0.629 \mu_0 \quad (2)$$

The average value of  $f/Q$  (0.09) was determined by using the bio-optical model in stations that have both measured  $R_{rs}$  and IOPs in Tokyo Bay, which is consistent with that in Mishra et al. [11]. Both  $a(\lambda)$  and  $b_b(\lambda)$  are the sum of the contributions of pure water and three optically active constituents in water: phytoplankton, non-algal particles and colored dissolved organic matter. The  $a(\lambda)$ , and  $b_b(\lambda)$  can be expressed as

$$a(\lambda) = a_w(\lambda) + a_{ph}(\lambda) + a_{NAP}(\lambda) + a_{CDOM}(\lambda) \quad (3)$$

$$b_b(\lambda) = b_{b,w}(\lambda) + b_{b,p}(\lambda) \quad (4)$$

where  $a_w(\lambda)$  were taken from Buiteveld et al. [67] and  $b_{b,w}(\lambda)$  were taken from Dall'Olmo et al. [63] and Morel [62]. The radiance just above water surface was related to the radiance just below water surface by a factor of 0.544 [68]. Hence, the remote sensing reflectance just above the water surface,  $R_{rs}(\lambda)$ , can be calculated as

$$R_{rs}(\lambda) = 0.049 \times \left( \frac{b_b(\lambda)}{a(\lambda) + b_b(\lambda)} \right) \quad (5)$$

**Table 2.** Symbols and definitions.

Symbol	Description	Units
(Chla)	Chlorophyll-a concentration	mg m <sup>-3</sup>
(NAP)	Non-algal particle concentration	g m <sup>-3</sup>
(CDOM)	Colored dissolved organic matter absorption at 440 nm	m <sup>-1</sup>
$a_w(\lambda)$	Absorption coefficient of pure water	m <sup>-1</sup>
$a_{ph}(\lambda)$	Absorption coefficient of phytoplankton	m <sup>-1</sup>
$a_{NAP}(\lambda)$	Absorption coefficient of NAP	m <sup>-1</sup>
$a_{CDOM}(\lambda)$	Absorption coefficient of CDOM	m <sup>-1</sup>
$a(\lambda)$	Total absorption coefficient (= $a_w(\lambda) + a_{ph}(\lambda) + a_{NAP}(\lambda) + a_{CDOM}(\lambda)$ )	m <sup>-1</sup>
$b_{b,w}(\lambda)$	Backscattering coefficients of pure water	m <sup>-1</sup>
$b_{b,p}(\lambda)$	Backscattering coefficients of suspended particles	m <sup>-1</sup>
$b_{b,ph}(\lambda)$	Backscattering coefficients of phytoplankton	m <sup>-1</sup>
$b_{b,NAP}(\lambda)$	Backscattering coefficients of NAP	m <sup>-1</sup>
$b_b(\lambda)$	Total backscattering coefficient (= $b_{b,w}(\lambda) + b_{b,ph}(\lambda) + b_{b,NAP}(\lambda)$ )	m <sup>-1</sup>
$R_{rs}(\lambda)$	Above-surface remote sensing reflectance	sr <sup>-1</sup>
$r_{rs}(\lambda)$	Subsurface remote sensing reflectance	sr <sup>-1</sup>

### 2.3. Simulating the Remote Sensing Reflectance

Researchers have proposed many models to generate simulated  $R_{rs}$  based on bio-optical models [47,69,70]. The key difference among these models is the parameters of specific absorption and backscattering [9]. The chlorophyll concentration and  $a_{ph}(\lambda)$  have a proportional relationship [71] that can be expressed as

$$a_{ph}(\lambda) = [Chla] \times a_{ph}^*(\lambda) \quad (6)$$

The NAP and CDOM have similar trends for absorption spectrum, which can be described as exponential decay function with increasing wavelength. The  $a_{NAP}(\lambda)$ , and  $a_{CDOM}(\lambda)$  are estimated from their reference values at 440-nm as follows:

$$a_{NAP}(\lambda) = [NAP] \times a_{NAP}^*(\lambda) = [NAP] \times a_{NAP}^*(440) \times e^{(-S_{NAP}(\lambda-440))} \quad (7)$$

$$a_{CDOM}(\lambda) = [CDOM] \times a_{CDOM}^*(\lambda) = [CDOM] \times a_{CDOM}^*(440) \times e^{(-S_{CDOM}(\lambda-440))} \quad (8)$$

where the values of  $a_{NAP}^*(440)$  and  $a_{CDOM}^*(440)$  were  $0.03483$  and  $1.0 \text{ m}^{-1}$ , respectively. The slopes  $S_{NAP}$  and  $S_{CDOM}$  equaled  $0.00899$  and  $0.01547$ , respectively. The backscattering coefficient of particles,  $b_{b,p}(\lambda)$ , at different wavelengths was estimated by fitting the measured backscattering at the six wavelengths with an exponential function:

$$b_{b,p}(\lambda) = b_{b,p}(550) \left( \frac{\lambda}{550} \right)^{-n} \quad (9)$$

where  $n$  stands for the spectral slope of  $b_{b,p}(\lambda)$  and  $b_{b,p}(550)$  refers to the backscattering at the 550 nm band. The values for  $b_{b,p}(550)$  and  $n$  were  $0.02141 \text{ m}^{-1}$  and  $1.25848$ , respectively. The segregation of  $b_{b,p}(\lambda)$  into the backscattering of phytoplankton ( $b_{b,ph}(\lambda)$ ) and non-algal particles ( $b_{b,NAP}(\lambda)$ ) was based on the assumption that their contributions to  $b_{b,p}(\lambda)$  were proportionally correlated to their concentrations [47]. Separating NAP from the TSS with laboratory analysis is impossible [72], so the approach of Gons et al. [73] was employed to divide the TSS into NAP and phytoplankton suspended solids (PSS). As a result, it was assumed that the  $1.0 \text{ mg m}^{-3}$  Chla concentration approximately equaled  $0.0687 \text{ g m}^{-3}$  TSS. The NAP concentration was calculated by subtracting the PSS ( $=0.0687 \times \text{Chla}$ ) from the TSS.

The reflectance caused by chlorophyll fluorescence emission for Case 2 waters was also considered as proposed by Gilerson et al. [71]. Fluorescence reflectance follows a Gaussian shape with a peak at 685 nm, a full-width half maximum of 25 nm and a standard deviation,  $\sigma$ , of 10.6 nm [74]. Thus, the chlorophyll fluorescence emission reflectance  $R_{rs,fl}(\lambda)$  was modeled as

$$R_{rs,fl}(\lambda) = \frac{fl(685)}{1000 \times E_d(685)} \times \exp \left[ -0.5 \times \left( \frac{\lambda - 685}{\sigma} \right)^2 \right] \quad (10)$$

where  $E_d(685)$  was  $1.1 \text{ W m}^{-2} \text{ nm}^{-1}$  under clear sky conditions Based on the Hydrolight simulation [71], and  $fl(685)$  is the chlorophyll fluorescence at 685 nm, which was calculated as

$$fl(685) = \frac{0.0375 [Chla]}{1 + 0.32 a_{CDOM}(440) + 0.01 [NAP] + 0.032 [Chla]} \quad (11)$$

The total remote sensing reflectance was generated as the sum of the reflectance in Equations (5) and (10) [11].

### 2.4. MERIS Images Processing

MERIS L1b products of 300 m full resolution from European Space Agency (ESA) Earthnet Online [75] were processed using BEAM V5.0 software (Envisat/Brockman Consult, Hamburg,

Germany). All clear and partially clear MERIS images that contain Lake Kasumigaura and matched the monthly field observations from 2002 to 2012 were extracted. The matchup process included all the images acquired at the same day or one-day difference from field observations. It was assumed that the changes in Chla concentrations within one day would not be significant due to the stability of weather conditions (e.g., wind speed) during that day (Table S1 in Supplementary Material). The matchup process resulted in a total of 13 images (i.e., five images at the same day and eight images within a one-day difference).

All images were pre-processed using a Smile Correction processor to adjust the variations in the spectral wavelengths among MERIS's five cameras and within the same camera [76]. In order to convert MERIS L1b top-of-atmosphere radiances to water-leaving reflectance, the Case-2 Regional (C2R), the Eutrophic Lake (EUL) and Boreal Lake (BL) processors are neural network modules for performing atmospheric correction in Case 2 waters [35,77]. The three processors share the same neural network atmospheric correction module, while the difference among them is the training data that used to trained inverse and forward coupled neural network to retrieve the IOPs and constituent concentrations from the atmospherically corrected reflectance [35,77]. During this study, the water-leaving reflectance is only needed from MERIS data, while the Chla concentrations will be taken from the matched field observations, not from the neural network modules. Thus, the EUL processor was employed to perform atmospheric correction [77]. The final number of matched stations decreased from 130 to 77 stations due to quality control flags in L1b product (e.g., invalid, bright, suspect, land, or glint risk) or during the atmospheric correction process. Figure 3 shows the water leaving reflectance of the 77 stations resulting from the matching process over Lake Kasumigaura.

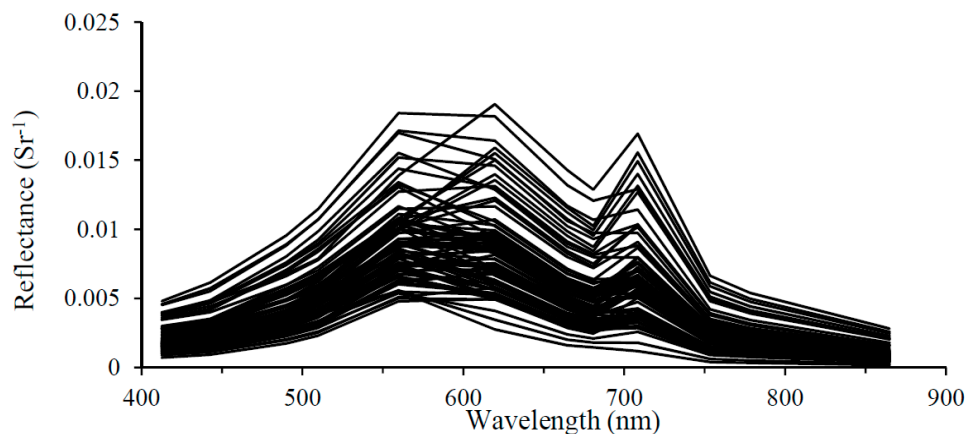


**Figure 3.** Atmospheric corrected remote sensing reflectance spectra for 77 stations matched the field observation in Lake Kasumigaura from 2002 to 2012.

### 2.5. Accuracy Assessment of the Algorithms

The retrieval accuracy was assessed using three indices: coefficient of determination ( $R^2$ ) [78] the root mean square error (RMSE) [79], and the mean absolute relative error (MARE) [79], as follows:

$$R^2 = \left[ \frac{N \times \sum_{i=1}^N (Chla_{i,meas} \times Chla_{i,retr}) - \sum_{i=1}^N Chla_{i,meas} \times \sum_{i=1}^N Chla_{i,retr}}{\sqrt{[N \times \sum_{i=1}^N (Chla_{i,meas})^2 - (\sum_{i=1}^N Chla_{i,meas})^2] [N \times \sum_{i=1}^N (Chla_{i,retr})^2 - (\sum_{i=1}^N Chla_{i,retr})^2]}} \right]^2 \quad (12)$$

$$RMSE = \sqrt{\frac{\sum_{i=1}^N (Chla_{i,meas} - Chla_{i,retr})^2}{N}} \quad (13)$$

$$MARE = \frac{1}{N} \times \sum_{i=1}^N \frac{|(Chla_{i,meas} - Chla_{i,retr})|}{Chla_{i,meas}} \times 100 \quad (14)$$

where  $Chla_{i,meas}$  and  $Chla_{i,retr}$  refer to the measured and retrieved Chla concentrations, respectively; and  $N$  is the total number of samples.

### 3. Construction of the Multi-Algorithm Indices and Look-Up Table (MAIN-LUT)

The proposed technique relies on creating a library of simulated reflectance dataset covering wide ranges of Chla, NAP and CDOM concentrations. The simulated reflectance dataset was generated based on the bio-optical model and specific inherent optical properties (SIOPs) from Tokyo Bay (Sections 2.2 and 2.3). The bio-optical modeling is used to link remote sensing reflectance with optically active constituents in the water column (i.e., Chla, NAP, and CDOM). By changing the concentration of any of these three constituents, remote sensing reflectance will change. Consequently, a simulated dataset of 500,000  $R_{rs}$  spectra was generated covering wide ranges of Chla (1–200  $\text{mg m}^{-3}$ ) (hereafter, reference Chla), NAP (1–200  $\text{g m}^{-3}$ ), and CDOM (1–10  $\text{m}^{-1}$ ) concentrations. Increments of 2.0  $\text{mg m}^{-3}$ , 2.0  $\text{g m}^{-3}$ , and 2.0  $\text{m}^{-1}$  were used for Chla, NAP and CDOM concentrations, respectively. Each of the generated  $R_{rs}$  spectra were tagged with the Chla, NAP, and CDOM concentrations, which were used during the generation of simulated  $R_{rs}$  spectra.

The major limitation to perform spectral matching with multi-spectral data is associated with the limited number of available bands, particularly when the bands of the blue spectrum were excluded due to difficulties in atmospheric correction for that part of the spectrum [80]. On the other hand, there was no relation between the reference Chla and individual bands of the multi-spectral data (e.g., 665-nm band) as shown in Figure S1 (Supplementary Material). Many algorithms have been proposed to retrieve Chla concentration in Case 2 waters [11,21,24,25]. These algorithms provide indices correlated with Chla concentrations [37]. Four algorithms were proposed for the proposed technique (i.e., 2-band ratio (Equation (15)), 3-band algorithm (Equation (16)), maximum chlorophyll index (Equation (17)) and normalized difference chlorophyll index (Equation (18)):

$$\text{Chla} \propto R_{rs}(\lambda_2) / R_{rs}(\lambda_1) \quad (15)$$

$$\text{Chla} \propto \left( R_{rs}^{-1}(\lambda_1) - R_{rs}^{-1}(\lambda_2) \right) * R_{rs}(\lambda_3) \quad (16)$$

$$\text{MCI} = R_{rs}(\lambda_2) - R_{rs}(\lambda_1) \left[ \frac{\lambda_2 - \lambda_1}{\lambda_3 - \lambda_1} R_{rs}(\lambda_3) - R_{rs}(\lambda_1) \right] \quad (17)$$

$$\text{Chla} \propto \left( R_{rs}(\lambda_2) - R_{rs}(\lambda_1) \right) / \left( R_{rs}(\lambda_2) + R_{rs}(\lambda_1) \right) \quad (18)$$

The wavelengths incorporated with each algorithm were summarized in Table 3. The eight algorithms mentioned in Table 3 represent the most accurate algorithms among 43 algorithms' combinations that were evaluated by Salem et al. [81] using measured and simulated datasets. In addition, these eight algorithms do not require hyperspectral  $R_{rs}$ . Scatter plots between the reference Chla and the above-mentioned algorithms with different wavelengths (Table S3) were performed (Figure 4). Investigated algorithms provided correlation with reference Chla: high correlation (e.g., 2b-[665, 709]), moderated correlation (e.g., 3b-[680, 709, 754]), and low correlation (e.g., MCI [680, 709, 754]) (Figure 4). Thus, the index of these algorithms could be used to retrieve Chla concentration of measured  $R_{rs}$  by comparing the index of measured  $R_{rs}$  with the indices of simulated  $R_{rs}$  to extract the simulated  $R_{rs}$  with the same index. The problem is that there are many simulated  $R_{rs}$  that have same measured index during the matchup process. Thus, multi-algorithm indices should be used to obtain the simulated  $R_{rs}$ , which is close to the measured  $R_{rs}$ .

**Table 3.** The incorporated band for each algorithm.

No.	Algorithms	Algorithms' Name	Wavelength			References
			$\lambda_1$	$\lambda_2$	$\lambda_3$	
1	Two-band ratio	2b [665, 709]	665	709		Gons [21]
2		2b [680, 709]	680	709		
3	Three-band algorithm	3b [665, 709, 754]	665	709	754	Dall'Olmo et al. [24]
4		3b [680, 709, 754]	680	709	754	
5	Maximum chlorophyll index	MCI [665, 709, 754]	665	709	754	Gower et al. [82]
6		MCI [680, 709, 754]	680	709	754	
7	Normalized difference chlorophyll index	NDCI [665, 709, 754]	665	709		Mishra et al. [11]
8		NDCI [680, 709, 754]	680	709		

Different combinations of these four algorithms were examined with the MAIN-LUT technique to find the best combination. Table 4 summarized eight combinations that were investigated. The flowchart in Figure 5 illustrates the concept of MAIN-LUT using the 2-indices-[665] combination as an example, whereas the major steps of the MAIN-LUT as follows:

- Step (0) two things should be prepared and selected before using MAIN-LUT: (1) a library of simulated  $R_{rs}$  should be provided through a look-up table; and (2) one combination of algorithms should be selected from Table 4. The selected combination is hereafter called Sample Combination through the coming steps.
- Step (1) calculating algorithms indices for the measured reflectance using Equations (15)–(18). The number of required indices relies on the selection of the Sample Combination in Step (0). For example, the 2-indices-[665] combination was selected in the flowchart (Figure 5). As a result, the indices of 2b-[665, 709] and 3b-[665, 709, 754] algorithms were estimated as  $(2b_{665}^{meas} = R_{rs}(709)/R_{rs}(665))$  and  $(3b_{665}^{meas} = [1/R_{rs}(665) - 1/R_{rs}(754)] * R_{rs}(754))$  as shown in Figure 5.
- Step (2) for each measured index estimated in Step (1), simulated reflectance spectra from a look-up table (LUT) that have the same index should be extracted. Of course, many simulated reflectance spectra with different tagged Chla will be extracted from this matching process. For example, the simulated reflectance  $(R_{rs,200}^{simu}, R_{rs,1520}^{simu})$  were extracted because they matched the  $3b_{665}^{meas}$ . The 200 and 1520 represent the tagged numbers of simulated reflectance for a certain combination of Chla, NAP, and CDOM and these tagged numbers range from 1 to 500,000.
- Step (3) grouping of simulated reflectance extracted from Step (2), which was generated from the matching process of each measured index.
- Step (4) estimating algorithm indices for each of simulated reflectance grouped in Step (3). The number of required indices is based on the Sample Combination selected in Step (0).
- Step (5) The RMSE is used to compare the indices of measured reflectance with simulated indices of each extracted reflectance in Step (3) as follows:

$$RMSE = \sqrt{\frac{\sum_{i=1}^n (Index_{i,meas} - Index_{i,simu}^j)^2}{n}} \quad (19)$$

where  $Index_{i,meas}$  denote measured indices (i.e.,  $2b_{665}^{meas}$  and  $3b_{665}^{meas}$  for 2b-indices-[665] combination);  $Index_{i,simu}^j$  refer to simulated indices calculated for each simulated  $R_{rs}$  spectrum (i.e.,  $(2b_{665}^{simu})^j$  and  $(3b_{665}^{simu})^j$  for 2b-indices-[665] combination),  $j$  is an index for simulated reflectance grouped in Step (3); and  $n$  represents the number of indices in the Sample Combination (i.e.,  $n = 2$  for 2b-indices-[665] combination). The minimum RMSE value represents

the closest simulated spectrum from the measured spectrum. As a result, the tagged Chla for that simulated  $R_{rs}$  will be the retrieved Chla concentration of the measured  $R_{rs}$ .

**Table 4.** Algorithms’ combination investigated with multi-algorithm indices and the look-up table (MAIN-LUT) technique.

Algorithms’ Combinations	Algorithms’ Name *							
	2b [665, 709]	2b [680, 709]	3b [665, 709, 754]	3b [680, 709, 754]	MCI [665, 709, 754]	MCI [680, 709, 754]	NDCI [665, 709]	NDCI [680, 709]
8-indices	✓	✓	✓	✓	✓	✓	✓	✓
6-indices	✓	✓	✓	✓			✓	✓
4-indices-[2b & 3b]	✓	✓	✓	✓				
4-indices-[665]	✓		✓		✓		✓	
3-indices-[665]	✓		✓				✓	
2-indices-[665]	✓		✓					
4-indices-[680]				✓		✓		
3-indices-[680]		✓		✓				✓

\* Wavelengths incorporated with each algorithm were summarized in Table 3.

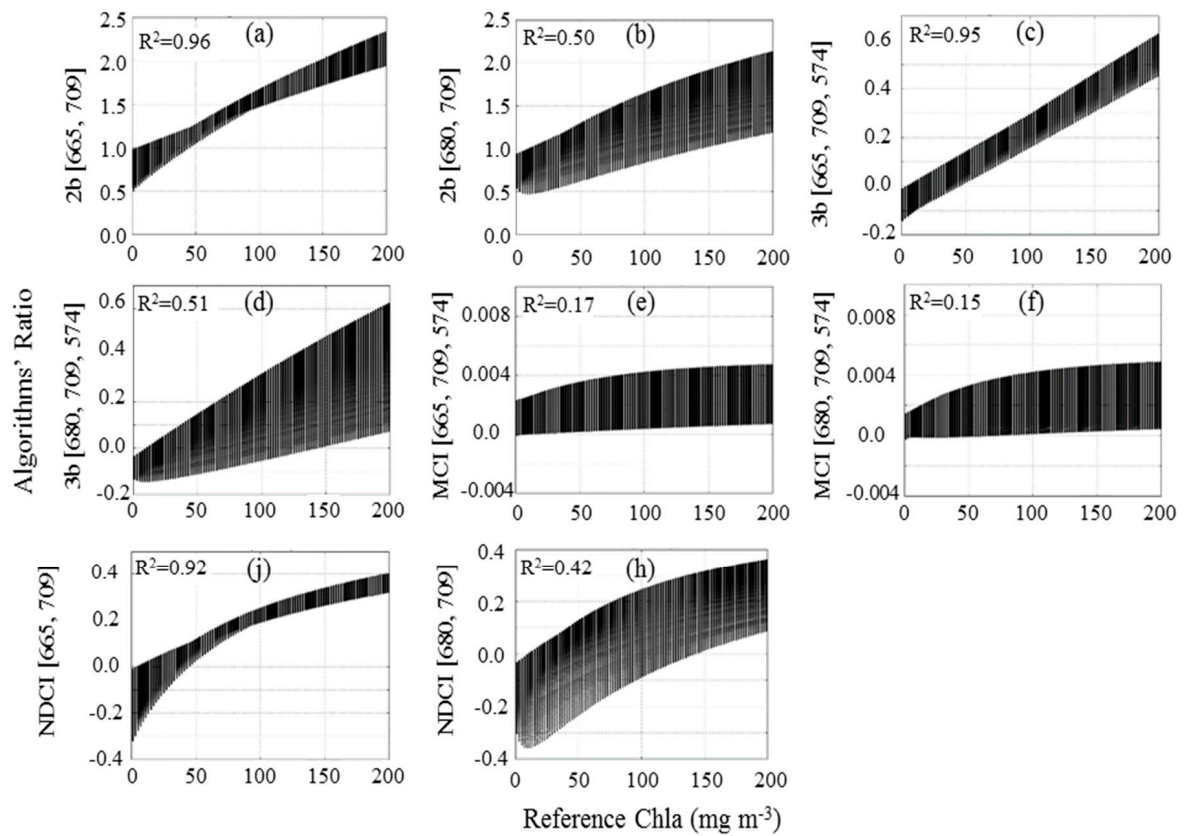


**Figure 4.** Scatter plots of reference Chla versus algorithms indices for the 500,000 simulated reflectance spectra. (a–h) represent indices of eight algorithms mentioned in Table 3.

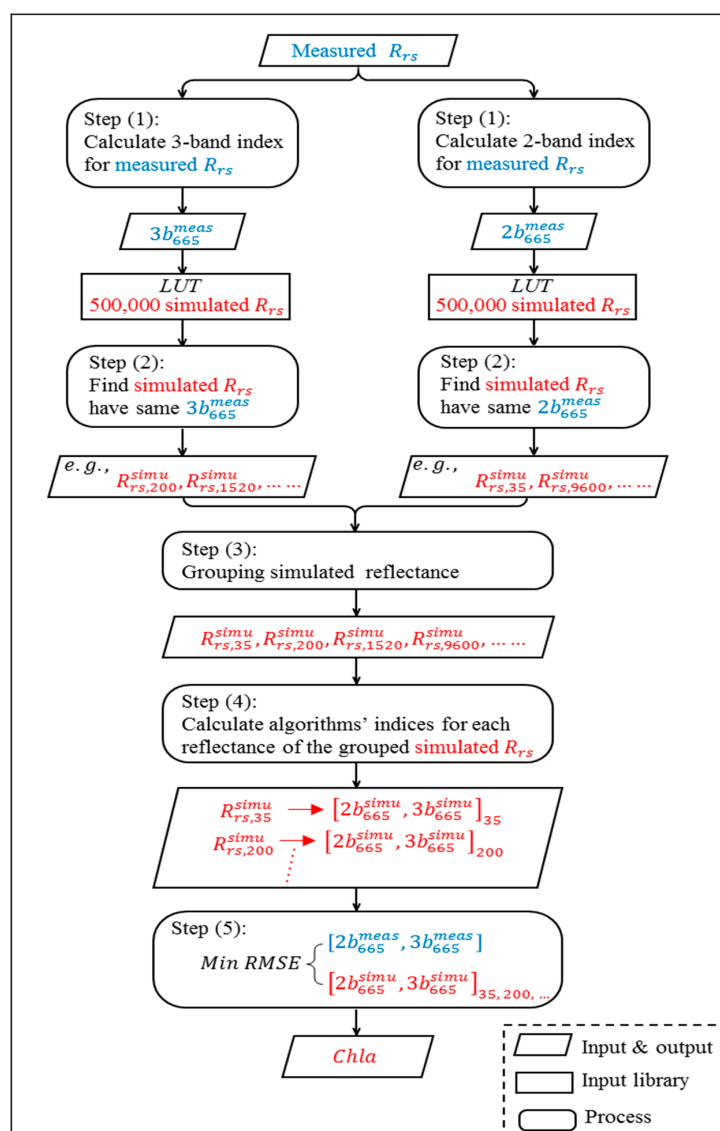


**Figure 5.** Concept and schematic flowchart of the multi-algorithm indices and the look-up table (MAIN-LUT) technique for the 2-indices-[665] combination. For other combinations in Table 4, a similar concept was employed.  $2b_{665}$  stands for 2b [665, 709] algorithm's index ( $= R_{rs}(709)/R_{rs}(665)$ );  $3b_{665}$  refers to the 3b [665, 709, 754] algorithm's index ( $= [1/R_{rs}(665) - 1/R_{rs}(754)] * R_{rs}(709)$ ); LUT represents the look-up table; numbers like 35 in  $R_{rs,35}^{simu}$  represents the tagged number for each simulated  $R_{rs}$  that range from 1 to 500,000; and *meas* and *simu* denote measured and simulated, respectively. The blue and red colors highlight the measured and simulated parameters, respectively.

## 4. Results and Discussion

### 4.1. Validation Using In Situ Measurements

The in situ data collected from Tokyo Bay between 2010 and 2013 (71 stations) were used to investigate the retrieval accuracy of the MAIN-LUT technique. The MAIN-LUT technique does not require a calibration process because Chla concentrations are directly retrieved from the look-up table. Therefore, all of the measured  $R_{rs}$  passed through the MAIN-LUT steps (from step 1 to step 5 as explained in previous section) to retrieve Chla concentrations. For the eight algorithms' combinations proposed in Table 4, the Chla concentrations for each combination were retrieved from the MAIN-LUT and compared with the measured Chla (Figure 6). In general, the results of MAIN-LUT revealed that most of algorithms'

combinations could accurately retrieve Chla concentrations (Figure 6). The 3-indices-[665] combination outperformed other combinations in terms of coefficient of determination ( $R^2$ ) of 0.692 with RMSE and MARE of  $21.4 \text{ mg m}^{-3}$  and 142.6%, respectively (Figure 6e). Overall, 3-indices-[665], 4-indices-[665], and 2-indices-[665] provided highest retrieval accuracy with average  $R^2$ , RMSE and MARE of 0.681,  $21.43 \text{ mg m}^{-3}$  and 141.87%, respectively. In contrast, 4-indices-[680] and 3-indices-[680] introduced the lowest averaged retrieval accuracy ( $R^2 = 0.277$ ,  $\text{RMSE} = 22.7 \text{ mg m}^{-3}$ ,  $\text{MARE} = 233.6\%$ ) (Figure 6g,h). This can be attributed to the fact that the 665 nm is located near the red Chla absorption maximum, which allow algorithms incorporated a 665 nm band to capture the variation of Chla better than that incorporated 680 nm band.

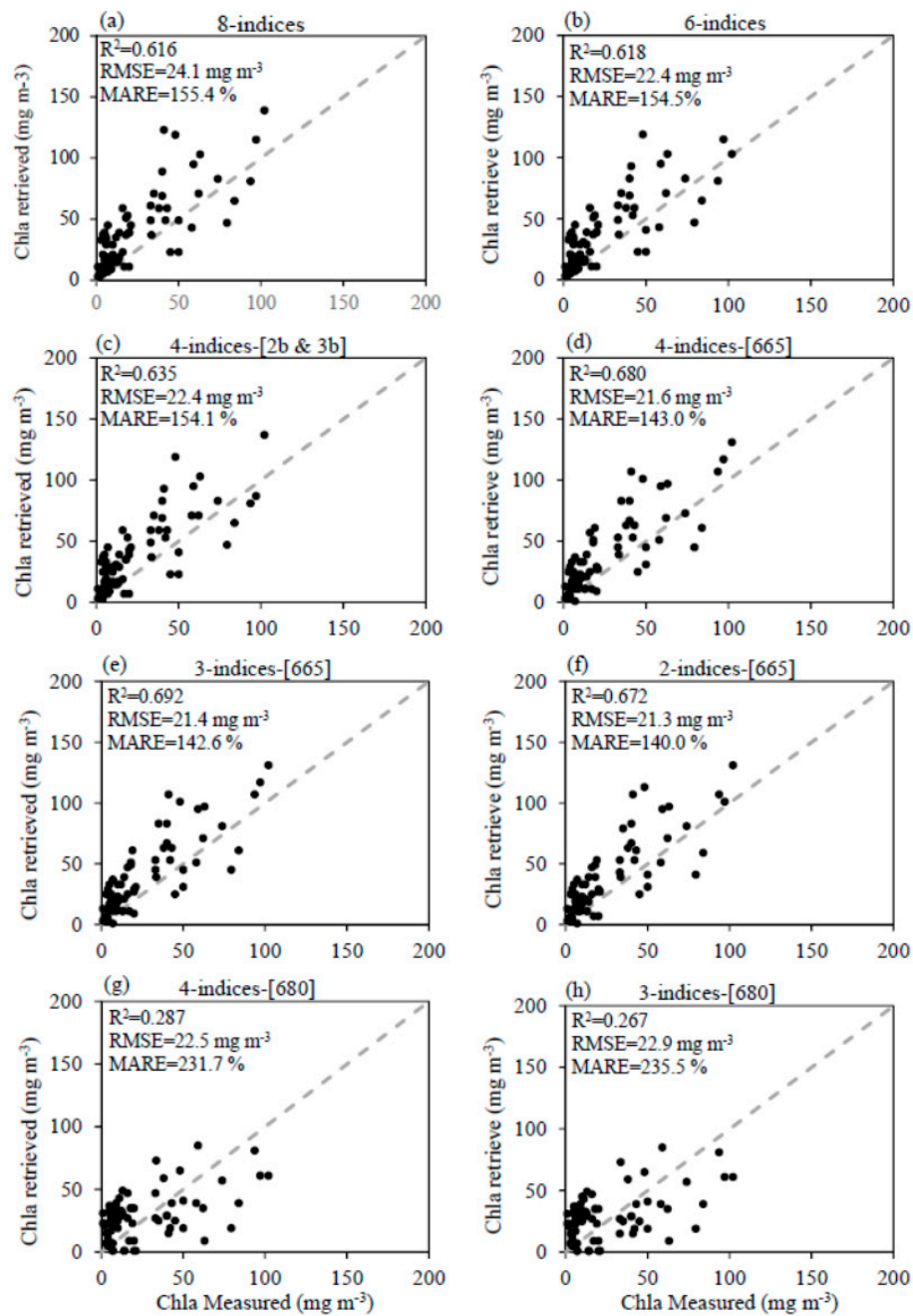


**Figure 6.** Validation plots between Chla measured in Tokyo Bay (71 stations collected between 2010 and 2013) and retrieved Chla from eight different algorithms' combinations assessed for MAIN-LUT. Algorithms used in each combination from (a) to (h) were mentioned in Table 4.

The performance of the MAIN-LUT was also examined with in situ measurements from Lake Kasumigaura collected in 2016 with total sampling points of 68 stations. Although the simulated  $R_{rs}$  data of the MAIN-LUT technique was generated based on IOP values from Tokyo Bay, the MAIN-LUT produced higher Chla retrieval accuracy for Lake Kasumigaura than Tokyo Bay for different algorithms' combinations (Figures 6 and 7). This result can be attributed to the fact that the four algorithms incorporated with MAIN-LUT (Equations (15)–(18)) are mainly developed for Case 2 waters with high Chla and TSS concentrations. Comparing the characteristics of these two water bodies revealed that water conditions in Lake Kasumigaura ( $\text{Chla} = 55.86 \text{ mg m}^{-3}$ ,  $\text{TSS} = 21.71 \text{ g m}^{-3}$ , Table 1) are more correlated with the algorithms' assumption than Tokyo Bay ( $\text{Chla} = 25.14 \text{ mg m}^{-3}$ ,  $\text{TSS} = 8.29 \text{ g m}^{-3}$ ). In addition, the MARE values for all combinations were very high for Tokyo Bay comparing with the same combinations at Lake Kasumigaura (Figures 6 and 7). The reason is mainly due to the fact that the MARE is a relative error that assesses the Chla retrieval over a relatively low range of Chla concentration in Tokyo Bay. As a result, any small difference between the measured and retrieved Chla concentrations would cause a high relative error.

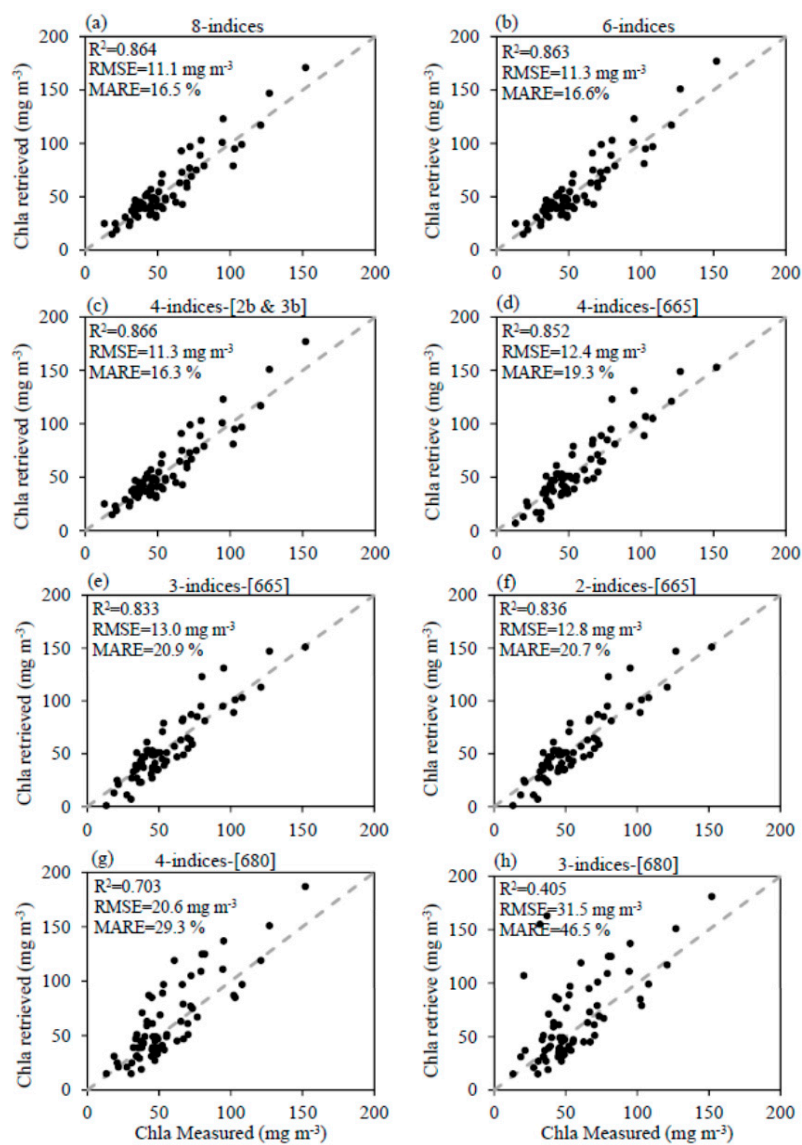


**Figure 7.** Validation plots between Chla measured in Lake Kasumigaura (68 stations collected in 2016) and retrieved Chla from different algorithms' combinations assessed for MAIN-LUT. Algorithms used in each combination from (a) to (h) were mentioned in Table 4.

The highest retrieval accuracy for Lake Kasumigaura was achieved by 4-indices-[2b & 3b] combination with  $R^2$  of 0.866, RMSE of  $11.3 \text{ mg m}^{-3}$ , and MARE of 16.3% (Figure 7c). The top three combinations in terms of Chla retrieval were 4-indices-[2b & 3b], 8-indices, and 6-indices with average  $R^2$ , RMSE, and MARE of 0.866,  $11.23 \text{ mg m}^{-3}$  and 16.47%, respectively. The second tier of algorithms' combinations were 3-indices-[665], 4-indices-[665], and 2-indices-[665] which introduced slightly high retrieval accuracy, with  $R^2$ , RMSE and MARE of 0.840,  $12.73 \text{ mg m}^{-3}$  and 20.3%, respectively. The retrieval accuracy of a 4-indices-[680] combination significantly improved in terms of  $R^2$  (from 0.287 to 0.703) and MARE (from 231.7 to 29.3%) (Figures 6g and 7g). The 3-indices-[680] combination was also improved compared with Tokyo Bay (Figures 6h and 7h).

#### 4.2. Validation Using MERIS Data

MAIN-LUT technique was also validated using MERIS sensor data. A matchup process executed between field observation campaigns in Lake Kasumigaura and MERIS images acquired at same day or one-day differences during 2002–2012, resulting in 130 matched stations. However, the final number of stations that was used during the validation process reduced to 77 stations (Table 1—Dataset 2), due to flags occurring through image processing. Therefore, MERIS reflectance spectra were used as an input for MAIN-LUT to retrieve Chla concentrations, which were compared with the measured Chla during the field campaigns. In general, all algorithms' combinations provided relatively acceptable Chla retrieval, even for 4-indices-[680] and 3-indices-[680], which introduced the lowest retrieval accuracy for Tokyo Bay and Lake Kasumigaura (Figure 8). This can be attributed to the fact that the neural network atmospheric correction module does not include the inelastic reflectance (e.g., fluorescence) for the simulated dataset that was used to train the module, which will affect the accuracy of the water-leaving reflectance of MERIS data in the red and near infrared (Red-NIR) regions of the spectrum [76].

The 4-indices-[680] provided the highest accuracy in terms of RMSE of  $28.9 \text{ mg m}^{-3}$ . Furthermore, the disruption of scatter plot of the 4-indices-[680] combination was close to a 1:1 line (Figure 8g) compared to most of the other combinations that underestimated Chla  $>50 \text{ mg m}^{-3}$  (Figure 8a–f). This is mainly due to the fact that the simulated dataset of the MAIN-LUT considered the fluorescence reflectance in contrast to the EUL atmospheric correcting module that neglected the fluorescence reflectance during the training process. Thus, the magnitude of atmospherically corrected reflectance, particularly in the Red-NIR, is lower than the simulated reflectance of MAIN-LUT for the same Chla concentration. The 2-indices-[665] outperformed other combinations with  $R^2$  of 0.57. The retrieval accuracy of 2-indices-[665], 3-indices-[665], and 4-indices-[665] were the highest combinations in terms of  $R^2$  and MARE ( $R^2 = 0.564$ , RMSE =  $32.47 \text{ mg m}^{-3}$ , MARE = 43.4%) (Figure 8d–f). However, the scatter plot distribution of 3-indices-[680] was also close to the 1:1 line (Figure 8h), and it produced the lowest retrieval accuracy ( $R^2 = 0.385$ , RMSE =  $37.8 \text{ mg m}^{-3}$ , MARE = 74.3%).

The MAIN-LUT technique was also applied to MERIS images (pixel by pixel) to retrieve and illustrate the spatial distribution of Chla concentration along Lake Kasumigaura. Figure 9a,b show the spatial distribution of Chla concentration for the Lake Kasumigaura using two MERIS images on July 2004 and May 2009. The Chla concentrations were relatively high (up to  $90 \text{ mg m}^{-3}$ ) on May 2009, compared with July 2004 (up to  $50 \text{ mg m}^{-3}$ ) as shown in Figure 9a,b, respectively. In order to check the accuracy of these results, the monthly measured Chla concentrations at two stations (i.e., Station 1 (St. 1) and Station 2 (St. 2)) during 2002–2011 were illustrated in Figure 9c. The measured Chla concentrations were low on July 2004 (St. 1 =  $32 \text{ mg m}^{-3}$ , St. 2 =  $13 \text{ mg m}^{-3}$ ) and relatively high on May 2009 (St. 1 =  $79 \text{ mg m}^{-3}$ , St. 2 =  $58 \text{ mg m}^{-3}$ ), which emphasized the ability of the MAIN-LUT technique to capture the spatial and temporal distribution of Chla concentration. In general, the Chla concentration of St. 1 was higher than that at St. 2 due to the nutrient-rich inflow from the Sakura River and the Hanamura River into the lake near St. 1.

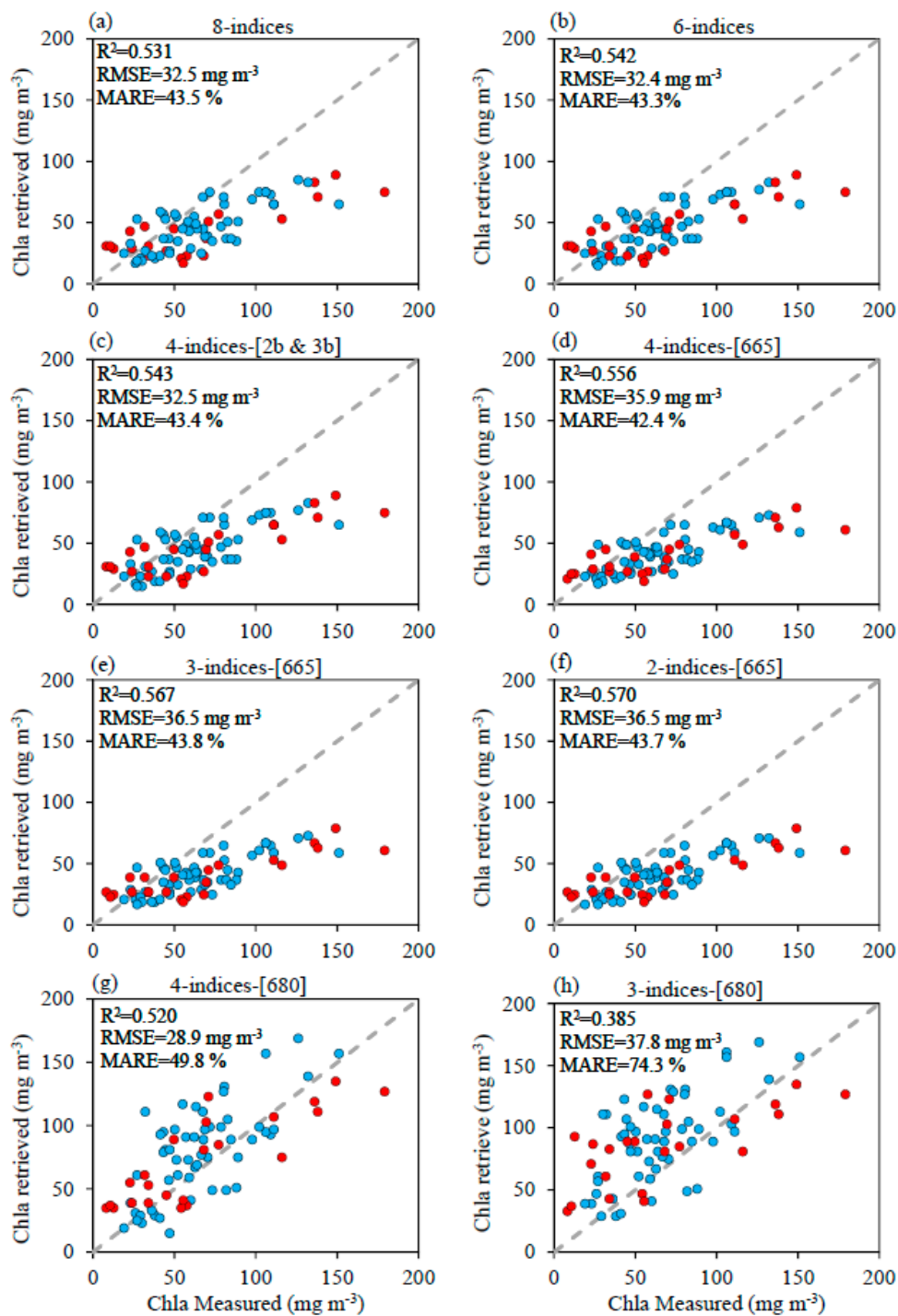


**Figure 8.** Validation plots between Chla measured in Lake Kasumigaura (77 stations matched Medium Resolution Imaging Spectrometer (MERIS) images and collected during 2002–2012) and retrieved Chla from different algorithms' combinations assessed for MAIN-LUT. The red and blue dots highlighted stations that matched MERIS images at same day and one-day differences, respectively. Algorithms used in each combination from (a) to (h) were mentioned in Table 4.

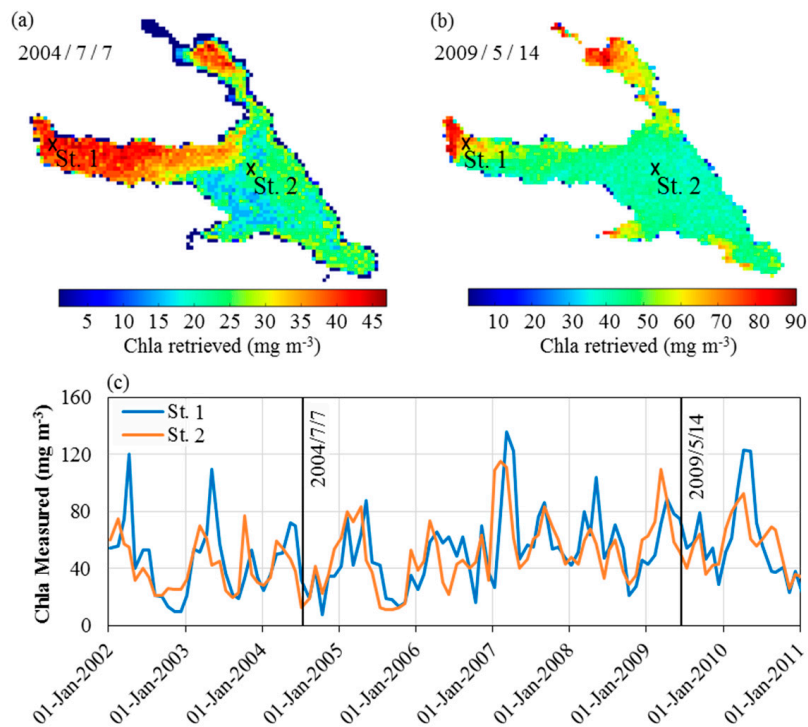


**Figure 9.** Spatial distribution of Chla concentration for Lake Kasumigaura was generated using MAIN-LUT for MERIS images on (a) 7 July 2004 and (b) 14 May 2009; and (c) the time series of monthly measured Chla concentration in Lake Kasumigaura at station 1 and station 2 from 2002 to 2011. The two black lines on the time series chart represent the dates of the two images.

#### 4.3. Comparing MAIN-LUT with Locally Tuned Algorithms

All algorithms incorporated with algorithms' combinations of MAIN-LUT (Table 4) were locally tuned and compared with MAIN-LUT. Each dataset (Tokyo Bay, Lake Kasumigaura datasets 1 and 2) shown in Table 1 was randomly divided to 70% and 30% for calibration and validation processes, respectively. Linear regression was adopted during the calibration process. Table 5 summarizes  $R^2$ , slope and intercept derived during the calibration process for each dataset. The results of the MAIN-LUT technique are not shown in Table 5 because the MAIN-LUT does not require the calibration stage. In general, the algorithm that provided the highest correlation varied among datasets (Table 5). The 3b [680, 709, 754], 3b [665, 709, 754], and 2b [680, 709] algorithms outperformed other algorithms for Tokyo Bay, Lake Kasumigaura dataset 1 and Lake Kasumigaura dataset 2, respectively. All algorithms of Lake Kasumigaura dataset 1 comparatively introduced higher correlation than that for Tokyo Bay. These results were mainly due to the fact that these algorithms are much more suitable for high-turbidity water in Lake Kasumigaura than Tokyo Bay.

The result from the validation process showed that the locally tuned algorithms provided slightly higher retrieval accuracy compared with MAIN-LUT technique (Table 6). However, the MAIN-LUT has two major advantages over the locally tuned algorithms: (1) the MAIN-LUT does not require the calibration process, and (2) the MAIN-LUT introduced comparatively high retrieval accuracy for in situ and satellite datasets, even with a look-up table generated from Tokyo Bay. Moreover, locally tuned algorithms produced different relationships for different datasets at the same algorithms, which emphasize the limitation of derived relationships to be applied for different locations or conditions.

**Table 5.** Algorithms' evaluation during the calibrations stage using Medium Resolution Imaging Spectrometer (MERIS) data.

Algorithms	Tokyo Bay (In Situ Data)			Lake Kasumigaura (Dataset 1)			Lake Kasumigaura (Dataset 2)		
	<i>n</i> = 49			<i>n</i> = 47			<i>n</i> = 53		
	R <sup>2</sup>	a <sub>0</sub>	a <sub>1</sub>	R <sup>2</sup>	a <sub>0</sub>	a <sub>1</sub>	R <sup>2</sup>	a <sub>0</sub>	a <sub>1</sub>
2b [665, 709]	0.67	68.52	−42.85	0.85	109.31	−81.19	0.52	143.98	−95.37
2b [680, 709]	0.61	126.25	−60.07	0.84	113.42	−88.35	<b>0.54</b>	<b>127.26</b>	<b>−93.89</b>
3b [665, 709, 754]	0.60	235.05	26.32	<b>0.91</b>	<b>267.05</b>	<b>26.95</b>	0.52	490.74	43.67
3b [680, 709, 754]	<b>0.67</b>	<b>464.98</b>	<b>64.40</b>	0.84	268.25	24.69	<b>0.54</b>	<b>358.01</b>	<b>35.77</b>
MCI [665, 709, 754]	0.66	55421.74	3.78	0.53	10289.16	10.44	0.06	7023.47	48.00
MCI [680, 709, 754]	0.65	94031.85	22.29	0.53	9633.17	18.75	0.07	6218.31	53.15
NDCI [665, 709]	0.61	130.19	27.76	0.83	273.10	24.10	0.48	356.96	48.64
NDCI [680, 709]	0.58	200.35	65.21	0.82	321.06	19.69	0.50	307.39	37.50

Data highlighted in bold represents the best algorithm performance with the highest R<sup>2</sup> during the calibration stage. Lake Kasumigaura Datasets 1 and 2 represent measurements collected in 2016 and during 2002–2012, respectively. a<sub>0</sub>, and a<sub>1</sub> represent slope and intercept for linear regression approach. The variable “N” denotes the number of samples used during the calibration stage.

**Table 6.** Algorithms' retrieval accuracies during the validation stage using MERIS data.

Algorithms	Tokyo Bay (In Situ Data)		Lake Kasumigaura (Dataset 1)		Lake Kasumigaura (Dataset 2)	
	<i>n</i> = 22		<i>n</i> = 21		<i>n</i> = 24	
	R <sup>2</sup>	RMSE	R <sup>2</sup>	RMSE	R <sup>2</sup>	RMSE
2b [665, 709]	0.67	15.42	0.85	7.65	0.52	28.99
2b [680, 709]	0.62	16.81	0.83	9.83	0.54	26.17
3b [665, 709, 754]	0.58	19.24	<b>0.89</b>	<b>8.49</b>	0.52	28.61
3b [680, 709, 754]	<b>0.70</b>	<b>17.51</b>	0.84	8.62	<b>0.55</b>	<b>27.81</b>
MCI [665, 709, 754]	0.68	15.35	0.51	23.93	0.08	33.96
MCI [680, 709, 754]	0.67	18.12	0.51	16.93	0.10	39.09
NDCI [665, 709]	0.63	14.04	0.84	9.51	0.50	19.70
NDCI [680, 709]	0.58	17.45	0.81	11.27	0.52	19.31
MAIN-LUT	0.69	21.40	0.85	11.3	0.57	36.50

Data highlighted in bold represents the best algorithm performance with the highest R<sup>2</sup>.

## 5. Conclusions

A multi-algorithm indices and look-up table (MAIN-LUT) technique was proposed to retrieve Chla concentration for optically complex Case 2 waters. The MAIN-LUT technique combines the advantage of a look-up table that covers wide ranges of trophic status with the ability of the existing Chla algorithms that provide indices correlated with Chla concentration. Multi-algorithms should be used to match algorithms' indices estimated from measured reflectance with the indices of simulated reflectance library. In situ measurements and MERIS data were used to validate MAIN-LUT over turbid and highly turbid water bodies. The results presented in this study reveal the ability of MAIN-LUT to accurately retrieve Chla concentration. Although the simulated dataset was generated based on IOPs from Tokyo Bay, the MAIN-LUT provided high retrieval accuracy for Lake Kasumigaura with in situ measurements and MERIS data. Eight algorithms' combinations were investigated for the MAIN-LUT. Six out of the eight combinations provided comparably high retrieval accuracy for Tokyo Bay (R<sup>2</sup> = 0.65, RMSE = 22.2 mg m<sup>−3</sup>, MARE = 148.27%), Lake Kasumigaura (R<sup>2</sup> = 0.85, RMSE = 11.98 mg m<sup>−3</sup>, MARE = 18.38%), and MERIS data (R<sup>2</sup> = 0.552, RMSE = 34.38 mg m<sup>−3</sup>, MARE = 43.35%). Accordingly, the 2-indices-[665] combination is proposed for MAIN-LUT. In addition, the 4-indices-[680] combination is recommended for MERIS data to overcome the limitation of other combinations, which underestimated the Chla concentration >50 mg m<sup>−3</sup>. The spatial and temporal distribution of Chla concentration was also captured using MAIN-LUT for MERIS images.

**Supplementary Materials:** The following are available online at <http://www.mdpi.com/2072-4292/9/6/556/s1>.

**Acknowledgments:** The first author would like to acknowledge the Japanese Government for providing the The Ministry of Education, Culture, Sports, Science and Technology (MEXT) scholarship to conduct this study. The authors thank the Japan Aerospace eXploration Agency (JAXA) for the Global Change Observation Mission for Climate (GCOM-C) RA2/4 funding.

**Author Contributions:** Salem Ibrahim Salem, Kazuo Oki and Hiroto Higa took part in the conception and designed the study; Hiroto Higa and Hiroshi Kobayashi performed the field measurements at Tokyo Bay; Komatsu Kazuhiro from the National Institute for Environmental Studies (NIES) performed the field measurements at Lake Kasumigaura between 2002–2012; Salem Ibrahim Salem performed the field measurements at Lake Kasumigaura in 2016; Salem Ibrahim Salem wrote the paper; Hyungjun Kim and Taikan Oki revised and commented the manuscript.

**Conflicts of Interest:** The authors declare no conflict of interest.

## References

1. Tyler, A.N.; Hunter, P.D.; Spyarakos, E.; Groom, S.; Constantinescu, A.M.; Kitchen, J. Developments in Earth observation for the assessment and monitoring of inland, transitional, coastal and shelf-sea waters. *Sci. Total Environ.* **2016**, *572*, 1307–1321. [[CrossRef](#)] [[PubMed](#)]
2. Bresciani, M.; Stroppiana, D.; Odermatt, D.; Morabito, G.; Giardino, C. Assessing remotely sensed chlorophyll-a for the implementation of the Water Framework Directive in European perialpine lakes. *Sci. Total Environ.* **2011**, *409*, 3083–3091. [[CrossRef](#)] [[PubMed](#)]
3. Shi, K.; Zhang, Y.; Liu, X.; Wang, M.; Qin, B. Remote sensing of diffuse attenuation coefficient of photosynthetically active radiation in Lake Taihu using MERIS data. *Remote Sens. Environ.* **2014**, *140*, 365–377. [[CrossRef](#)]
4. Austin, R.W.; Petzold, T.J. The Determination of the Diffuse Attenuation Coefficient of Sea Water Using the Coastal Zone Color Scanner. In *Oceanography from Space*; Barale, V., Gower, J.F.R., Alberotanza, L., Eds.; Springer: Boston, MA, USA, 1981; pp. 239–256.
5. Yoder, J.A.; McClain, C.R.; Blanton, J.O.; Oeymay, L.-Y. Spatial scales in CZCS-chlorophyll imagery of the southeastern U.S. continental shelf. *Limnol. Oceanogr.* **1987**, *32*, 929–941. [[CrossRef](#)]
6. International Ocean Colour Coordinating Group (IOCCG). *Remote Sensing of Inherent Optical Properties: Fundamentals, Tests of Algorithms, and Applications*; Lee, Z.-P., Ed.; Reports of the International Ocean Colour Coordinating Group; IOCCG: Dartmouth, NS, Canada, 2006; Volume 5.
7. International Ocean Colour Coordinating Group (IOCCG). *Phytoplankton Functional Types from Space*; Sathyendranath, S., Ed.; Reports of the International Ocean Colour Coordinating Group; IOCCG: Dartmouth, NS, Canada, 2014; Volume 15.
8. International Ocean Colour Coordinating Group (IOCCG). *Atmospheric Correction for Remotely-Sensed Ocean-Colour Products*; Reports of the International Ocean Colour Coordinating Group; Wang, M., Ed.; IOCCG: Dartmouth, NS, Canada, 2010; Volume 10.
9. Kutser, T. Quantitative detection of chlorophyll in cyanobacterial blooms by satellite remote sensing. *Limnol. Oceanogr.* **2004**, *49*, 2179–2189. [[CrossRef](#)]
10. Majazi, N.P.; Salama, M.S.; Bernard, S.; Harper, D.M.; Habte, M.G. Remote sensing of euphotic depth in shallow tropical inland waters of Lake Naivasha using MERIS data. *Remote Sens. Environ.* **2014**, *148*, 178–189. [[CrossRef](#)]
11. Mishra, S.; Mishra, D.R. Normalized difference chlorophyll index: A novel model for remote estimation of chlorophyll-a concentration in turbid productive waters. *Remote Sens. Environ.* **2012**, *117*, 394–406. [[CrossRef](#)]
12. Matsushita, B.; Yang, W.; Chang, P.; Yang, F.; Fukushima, T. A simple method for distinguishing global Case-1 and Case-2 waters using SeaWiFS measurements. *ISPRS J. Photogramm. Remote Sens.* **2012**, *69*, 74–87. [[CrossRef](#)]
13. Lee, Z.; Carder, K.L.; Arnone, R.A. Deriving Inherent Optical Properties from Water Color: A Multiband Quasi-Analytical Algorithm for Optically Deep Waters. *Appl. Opt.* **2002**, *41*, 5755. [[CrossRef](#)] [[PubMed](#)]
14. Garver, S.A.; Siegel, D.A. Inherent optical property inversion of ocean color spectra and its biogeochemical interpretation: 1. Time series from the Sargasso Sea. *J. Geophys. Res. Ocean.* **1997**, *102*, 18607–18625. [[CrossRef](#)]
15. O'Reilly, J.E.; Maritorena, S.; Mitchell, B.G.; Siegel, D.A.; Carder, K.L.; Garver, S.A.; Kahru, M.; McClain, C. Ocean color chlorophyll algorithms for SeaWiFS. *J. Geophys. Res.* **1998**, *103*, 24937. [[CrossRef](#)]

16. Li, L.; Li, L.; Song, K.; Li, Y.; Tedesco, L.P.; Shi, K.; Li, Z. An inversion model for deriving inherent optical properties of inland waters: Establishment, validation and application. *Remote Sens. Environ.* **2013**, *135*, 150–166. [[CrossRef](#)]
17. Song, K.; Li, L.; Tedesco, L.P.P.; Li, S.; Duan, H.; Liu, D.; Hall, B.E.E.; Du, J.; Li, Z.; Shi, K.; Zhao, Y. Remote estimation of chlorophyll-a in turbid inland waters: Three-band model versus GA-PLS model. *Remote Sens. Environ.* **2013**, *136*, 342–357. [[CrossRef](#)]
18. Sun, D.; Li, Y.; Le, C.; Shi, K.; Huang, C.; Gong, S.; Yin, B. A semi-analytical approach for detecting suspended particulate composition in complex turbid inland waters (China). *Remote Sens. Environ.* **2013**, *134*, 92–99. [[CrossRef](#)]
19. Yang, W.; Matsushita, B.; Chen, J.; Fukushima, T. A Relaxed Matrix Inversion Method for Retrieving Water Constituent Concentrations in Case II Waters: The Case of Lake Kasumigaura, Japan. *IEEE Trans. Geosci. Remote Sens.* **2011**, *49*, 3381–3392. [[CrossRef](#)]
20. Han, L.; Rundquist, D.C.; Liu, L.L.; Fraser, R.N.; Schalles, J.F. The spectral responses of algal chlorophyll in water with varying levels of suspended sediment. *Int. J. Remote Sens.* **1994**, *15*, 3707–3718. [[CrossRef](#)]
21. Gons, H.J. Optical Teledetection of Chlorophyll a in Turbid Inland Waters. *Environ. Sci. Technol.* **1999**, *33*, 1127–1132. [[CrossRef](#)]
22. Oki, K.; Yasuoka, Y. Estimation of Chlorophyll-a Concentration in Rich Chlorophyll Water Area from Near-infrared and Red Spectral Signature. *J. Remote Sens. Soc. Jpn.* **1996**, *16*, 315–323.
23. Oki, K.; Yasuoka, Y. Estimation of Chlorophyll Concentration in Lakes and Inland Seas with a Field Spectroradiometer above the Water Surface. *Appl. Opt.* **2002**, *41*, 6463. [[CrossRef](#)] [[PubMed](#)]
24. Dall’Olmo, G.; Gitelson, A.A.; Rundquist, D.C. Towards a unified approach for remote estimation of chlorophyll-a in both terrestrial vegetation and turbid productive waters. *Geophys. Res. Lett.* **2003**, *30*, 1938. [[CrossRef](#)]
25. Le, C.; Li, Y.; Zha, Y.; Sun, D.; Huang, C.; Lu, H. A four-band semi-analytical model for estimating chlorophyll a in highly turbid lakes: The case of Taihu Lake, China. *Remote Sens. Environ.* **2009**, *113*, 1175–1182. [[CrossRef](#)]
26. Lyu, H.; Li, X.; Wang, Y.; Jin, Q.; Cao, K.; Wang, Q.; Li, Y. Evaluation of chlorophyll-a retrieval algorithms based on MERIS bands for optically varying eutrophic inland lakes. *Sci. Total Environ.* **2015**, *530–531*, 373–382. [[CrossRef](#)] [[PubMed](#)]
27. Lee, Z.; Carder, K.L.; Mobley, C.D.; Steward, R.G.; Patch, J.S. Hyperspectral remote sensing for shallow waters: 2 Deriving bottom depths and water properties by optimization. *Appl. Opt.* **1999**, *38*, 3831. [[CrossRef](#)] [[PubMed](#)]
28. Klonowski, W.M.; Fearn, P.R.; Lynch, M.J. Retrieving key benthic cover types and bathymetry from hyperspectral imagery. *J. Appl. Remote Sens.* **2007**, *1*, 11505. [[CrossRef](#)]
29. Hedley, J.; Roelfsema, C.; Phinn, S.R. Efficient radiative transfer model inversion for remote sensing applications. *Remote Sens. Environ.* **2009**, *113*, 2527–2532. [[CrossRef](#)]
30. Brando, V.E.; Anstee, J.M.; Wettle, M.; Dekker, A.G.; Phinn, S.R.; Roelfsema, C. A physics based retrieval and quality assessment of bathymetry from suboptimal hyperspectral data. *Remote Sens. Environ.* **2009**, *113*, 755–770. [[CrossRef](#)]
31. Louchard, E.M.; Reid, R.P.; Stephens, F.C.; Davis, C.O.; Leathers, R.A.; Downes, T.V. *Optical Remote Sensing of Benthic Habitats and Bathymetry in Coastal Environments at Lee Stocking Island, Bahamas: A Comparative Spectral Classification Approach*; DTIC: Fort Belvoir, VA, USA, 2002.
32. Mobley, C.D.; Sundman, L.K.; Davis, C.O.; Bowles, J.H.; Downes, T.V.; Leathers, R.A.; Montes, M.J.; Bissett, W.P.; Kohler, D.D.R.; Reid, R.P.; et al. Interpretation of hyperspectral remote-sensing imagery by spectrum matching and look-up tables. *Appl. Opt.* **2005**, *44*, 3576. [[CrossRef](#)] [[PubMed](#)]
33. Doerffer, R.; Helmut, S. Neural network for retrieval of concentrations of water constituents with the possibility of detecting exceptional out of scope spectra. In Proceedings of the IGARSS 2000: IEEE 2000 International Geoscience and Remote Sensing Symposium, Honolulu, HI, USA, 24–28 July 2000; IEEE: Piscataway, NJ, USA, 2000.; Volume 2, pp. 714–717.
34. Baruah, P.J.; Tamura, M.; Oki, K.; Nishimura, H. Neural network modeling of lake surface chlorophyll and sediment content from Landsat TM imagery. In Proceedings of the Paper presented at the 22nd Asian Conference on Remote Sensing, Singapore, 5–9 November 2001; Volume 5, p. 9.
35. Doerffer, R.; Schiller, H. The MERIS Case 2 water algorithm. *Int. J. Remote Sens.* **2007**, *28*, 517–535. [[CrossRef](#)]

36. Shen, F.; Zhou, Y.-X.; Li, D.-J.; Zhu, W.-J.; Suhyb Salama, M. Medium resolution imaging spectrometer (MERIS) estimation of chlorophyll-a concentration in the turbid sediment-laden waters of the Changjiang (Yangtze) Estuary. *Int. J. Remote Sens.* **2010**, *31*, 4635–4650. [[CrossRef](#)]
37. Zhang, F.; Li, J.; Shen, Q.; Zhang, B.; Wu, C.; Wu, Y.; Wang, G.; Wang, S.; Lu, Z. Algorithms and Schemes for Chlorophyll a Estimation by Remote Sensing and Optical Classification for Turbid Lake Taihu, China. *IEEE J. Sel. Top. Appl. Earth Obs. Remote Sens.* **2015**, *8*, 350–364. [[CrossRef](#)]
38. Oki, K. Why is the Ratio of Reflectivity Effective for Chlorophyll Estimation in the Lake Water? *Remote Sens.* **2010**, *2*, 1722–1730. [[CrossRef](#)]
39. Carder, K.L.; Chen, F.R.; Lee, Z.P.; Hawes, S.K.; Kamykowski, D. Semianalytic Moderate-Resolution Imaging Spectrometer algorithms for chlorophyll a and absorption with bio-optical domains based on nitrate-depletion temperatures. *J. Geophys. Res.* **1999**, *104*, 5403. [[CrossRef](#)]
40. Huang, Y.; Jiang, D.; Zhuang, D.; Fu, J. Evaluation of hyperspectral indices for chlorophyll-a concentration estimation in Tangxun Lake (Wuhan, China). *Int. J. Environ. Res. Public Health* **2010**, *7*, 2437–2451. [[CrossRef](#)] [[PubMed](#)]
41. Zhou, L.; Roberts, D.A.; Ma, W.; Zhang, H.; Tang, L. Estimation of higher chlorophylla concentrations using field spectral measurement and HJ-1A hyperspectral satellite data in Dianshan Lake, China. *ISPRS J. Photogramm. Remote Sens.* **2014**, *88*, 41–47. [[CrossRef](#)]
42. Shi, K.; Li, Y.; Li, L.; Lu, H.; Song, K.; Liu, Z.; Xu, Y.; Li, Z. Remote chlorophyll-a estimates for inland waters based on a cluster-based classification. *Sci. Total Environ.* **2013**, *444*, 1–15. [[CrossRef](#)] [[PubMed](#)]
43. Gurlin, D.; Gitelson, A.A.; Moses, W.J. Remote estimation of chl-a concentration in turbid productive waters—Return to a simple two-band NIR-red model? *Remote Sens. Environ.* **2011**, *115*, 3479–3490. [[CrossRef](#)]
44. Matsushita, B.; Yang, W.; Yu, G.; Oyama, Y.; Yoshimura, K.; Fukushima, T. A hybrid algorithm for estimating the chlorophyll-a concentration across different trophic states in Asian inland waters. *ISPRS J. Photogramm. Remote Sens.* **2015**, *102*, 28–37. [[CrossRef](#)]
45. Kutser, T.; Metsamaa, L.; Strömbeck, N.; Vahtmäe, E. Monitoring cyanobacterial blooms by satellite remote sensing. *Estuar. Coast. Shelf Sci.* **2006**, *67*, 303–312. [[CrossRef](#)]
46. Matthews, M.W. A current review of empirical procedures of remote sensing in inland and near-coastal transitional waters. *Int. J. Remote Sens.* **2011**, *32*, 6855–6899. [[CrossRef](#)]
47. Yang, W.; Matsushita, B.; Chen, J.; Fukushima, T. Estimating constituent concentrations in case II waters from MERIS satellite data by semi-analytical model optimizing and look-up tables. *Remote Sens. Environ.* **2011**, *115*, 1247–1259. [[CrossRef](#)]
48. Lee, Z.; Carder, K.L.; Mobley, C.D.; Steward, R.G.; Patch, J.S. Hyperspectral remote sensing for shallow waters. I. A semianalytical model. *Appl. Opt.* **1998**, *37*, 6329–6338. [[CrossRef](#)] [[PubMed](#)]
49. Giardino, C.; Brando, V.E.; Dekker, A.G.; Strömbeck, N.; Candiani, G. Assessment of water quality in Lake Garda (Italy) using Hyperion. *Remote Sens. Environ.* **2007**, *109*, 183–195. [[CrossRef](#)]
50. Lyons, M.; Phinn, S.; Roelfsema, C. Integrating Quickbird Multi-Spectral Satellite and Field Data: Mapping Bathymetry, Seagrass Cover, Seagrass Species and Change in Moreton Bay, Australia in 2004 and 2007. *Remote Sens.* **2011**, *3*, 42–64. [[CrossRef](#)]
51. Lee, Z.; Carder, K.L.; Chen, R.F.; Peacock, T.G. Properties of the water column and bottom derived from Airborne Visible Infrared Imaging Spectrometer (AVIRIS) data. *J. Geophys. Res. Ocean.* **2001**, *106*, 11639–11651. [[CrossRef](#)]
52. Schueler, C.; Yoder, J.; Antoine, D.; Castillo, C.; Evans, R.; Mengelt, C.; Mobley, C.; Sarmiento, J.; Sathyendranath, S.; Siegel, D.; et al. Assessing Requirements for Sustained Ocean Color Research and Observations. In Proceedings of the AIAA SPACE 2011 Conference & Exposition, Long Beach, CA, USA, 27–29 September 2011; American Institute of Aeronautics and Astronautics: Reston, VA, USA, 2011.
53. Dekker, A.G.; Phinn, S.R.; Anstee, J.; Bissett, P.; Brando, V.E.; Casey, B.; Fearn, P.; Hedley, J.; Klonowski, W.; Lee, Z.P. Intercomparison of shallow water bathymetry, hydro-optics, and benthos mapping techniques in Australian and Caribbean coastal environments. *Limnol. Oceanogr. Methods* **2011**, *9*, 396–425. [[CrossRef](#)]
54. Dalponte, M.; Bruzzone, L.; Gianelle, D. Tree species classification in the Southern Alps based on the fusion of very high geometrical resolution multispectral/hyperspectral images and LiDAR data. *Remote Sens. Environ.* **2012**, *123*, 258–270. [[CrossRef](#)]
55. Lesser, M.P.; Mobley, C.D. Bathymetry, water optical properties, and benthic classification of coral reefs using hyperspectral remote sensing imagery. *Coral Reefs* **2007**, *26*, 819–829. [[CrossRef](#)]

56. NIES Lake Kasumigaura Database, National Institute for Environmental Studies, Japan. Available online: <http://db.cger.nies.go.jp/gem/moni-e/inter/GEMS/database/kasumi/index.html> (accessed on 20 November 2016).
57. Welschmeyer, N.A. Fluorometric analysis of chlorophyll a in the presence of chlorophyll b and pheopigments. *Limnol. Oceanogr.* **1994**, *39*, 1985–1992. [[CrossRef](#)]
58. Suzuki, R.; Ishimaru, T. An improved method for the determination of phytoplankton chlorophyll using *N,N*-dimethylformamide. *J. Oceanogr. Soc. Jpn.* **1990**, *46*, 190–194. [[CrossRef](#)]
59. American Public Health Association. *Standard Methods for the Examination of Water and Wastewater*; American Public Health Association: Washington, DC, USA, 2005.
60. Mobley, C.D. Estimation of the Remote-Sensing Reflectance from Above-Surface Measurements. *Appl. Opt.* **1999**, *38*, 7442–7448. [[CrossRef](#)] [[PubMed](#)]
61. Mitchell, B.G.; Kahru, M.; Wieland, J.; Stramska, M.; Mueller, J.L. Determination of spectral absorption coefficients of particles, dissolved material and phytoplankton for discrete water samples. *Ocean Opt. Protoc. Satell. Ocean Color Sens. Valid. Revis.* **2002**, *3*, 231–257.
62. Morel, A. Optical properties of pure water and pure sea water. *Opt. Asp. Oceanogr.* **1974**, *1*, 1–24.
63. Dall’Olmo, G.; Gitelson, A.A. Effect of bio-optical parameter variability and uncertainties in reflectance measurements on the remote estimation of chlorophyll-a concentration in turbid productive waters: Modeling results. *Appl. Opt.* **2006**, *45*, 3577. [[CrossRef](#)] [[PubMed](#)]
64. Mélin, F.; Vantrepotte, V.; Clerici, M.; D’Alimonte, D.; Zibordi, G.; Berthon, J.-F.; Canuti, E. Multi-sensor satellite time series of optical properties and chlorophyll-a concentration in the Adriatic Sea. *Prog. Oceanogr.* **2011**, *91*, 229–244. [[CrossRef](#)]
65. Gordon, H.; Brown, J.; Brown, O.; Evans, R.; Smith, R. A semianalytic radiance model of ocean color. *J. Geophys. Res.* **1988**, *93*, 10909–10924. [[CrossRef](#)]
66. Kirk, J.T.O. Dependence of relationship between inherent and apparent optical properties of water on solar altitude. *Limnol. Oceanogr.* **1984**, *29*, 350–356. [[CrossRef](#)]
67. Buiteveld, H.; Hakvoort, J.H.M.; Donze, M. Optical properties of pure water. In *Ocean Optics XII*; Jaffe, J.S., Ed.; International Society for Optics and Photonics: Bellingham, WA, USA, 1994; pp. 174–183.
68. Austin, R.W. Gulf of Mexico, ocean-color surface-truth measurements. *Bound. Layer Meteorol.* **1980**, *18*, 269–285. [[CrossRef](#)]
69. Zhu, W.; Yu, Q.; Tian, Y.Q.; Becker, B.L.; Zheng, T.; Carrick, H.J. An assessment of remote sensing algorithms for colored dissolved organic matter in complex freshwater environments. *Remote Sens. Environ.* **2014**, *140*, 766–778. [[CrossRef](#)]
70. Yang, W.; Matsushita, B.; Chen, J.; Yoshimura, K.; Fukushima, T. Retrieval of Inherent Optical Properties for Turbid Inland Waters From Remote-Sensing Reflectance. *IEEE Trans. Geosci. Remote Sens.* **2013**, *51*, 3761–3773. [[CrossRef](#)]
71. Gilerson, A.; Zhou, J.; Hlaing, S.; Ioannou, I.; Schalles, J.; Gross, B.; Moshary, F.; Ahmed, S. Fluorescence component in the reflectance spectra from coastal waters. Dependence on water composition. *Opt. Express* **2007**, *15*, 15702–15721. [[CrossRef](#)] [[PubMed](#)]
72. Oyama, Y.; Matsushita, B.; Fukushima, T.; Matsushige, K.; Imai, A. Application of spectral decomposition algorithm for mapping water quality in a turbid lake (Lake Kasumigaura, Japan) from Landsat TM data. *ISPRS J. Photogramm. Remote Sens.* **2009**, *64*, 73–85. [[CrossRef](#)]
73. Gons, H.J.; Burger-Wiersma, T.; Otten, J.H.; Rijkeboer, M. Coupling of phytoplankton and detritus in a shallow, eutrophic lake (Lake Loosdrecht, The Netherlands). *Hydrobiologia* **1992**, *233*, 51–59. [[CrossRef](#)]
74. Gower, J.F.R.; Doerffer, R.; Borstad, G.A. Interpretation of the 685 nm peak in water-leaving radiance spectra in terms of fluorescence, absorption and scattering, and its observation by MERIS. *Int. J. Remote Sens.* **1999**, *20*, 1771–1786. [[CrossRef](#)]
75. European Space Agency (ESA) Earthnet. Available Online: <http://earth.esa.int/> (accessed on 10 March 2015).
76. Binding, C.E.; Greenberg, T.A.; Jerome, J.H.; Bukata, R.P.; Letourneau, G. An assessment of MERIS algal products during an intense bloom in Lake of the Woods. *J. Plankton Res.* **2011**, *33*, 793–806. [[CrossRef](#)]
77. Doerffer, R.; Schiller, H. *MERIS Lake Water Algorithm for BEAM—MERIS Algorithm Theoretical Basis Document*; V1.0, 10 June 2008; GKSS Research Center: Geesthacht, Germany, 2008.
78. Egghe, L.; Leydesdorff, L. The relation between Pearson’s correlation coefficient  $r$  and Salton’s cosine measure. *J. Am. Soc. Inf. Sci. Technol.* **2009**, *60*, 1027–1036. [[CrossRef](#)]

79. Moore, T.S.; Dowell, M.D.; Bradt, S.; Verdu, A.R. An optical water type framework for selecting and blending retrievals from bio-optical algorithms in lakes and coastal waters. *Remote Sens. Environ.* **2014**, *143*, 97–111. [[CrossRef](#)] [[PubMed](#)]
80. Le, C.; Hu, C.; Cannizzaro, J.; English, D.; Muller-Karger, F.; Lee, Z. Evaluation of chlorophyll-a remote sensing algorithms for an optically complex estuary. *Remote Sens. Environ.* **2013**, *129*, 75–89. [[CrossRef](#)]
81. Salem, S.I.; Higa, H.; Kim, H.; Kobayashi, H.; Oki, K.; Oki, T. Retrieval accuracy assessment of chlorophyll-a algorithms considering different trophic statuses and optimal bands. *J. Great Lakes Res.* **2017**, in press.
82. Gower, J.; King, S.; Borstad, G.; Brown, L. Detection of intense plankton blooms using the 709 nm band of the MERIS imaging spectrometer. *Int. J. Remote Sens.* **2005**, *26*, 2005–2012. [[CrossRef](#)]



© 2017 by the authors. Licensee MDPI, Basel, Switzerland. This article is an open access article distributed under the terms and conditions of the Creative Commons Attribution (CC BY) license (<http://creativecommons.org/licenses/by/4.0/>).